INSTITUTE FOR DEFENSE ANALYSES

Comparison of Rising Resonator Relative Permittivity Measurements to Ground Penetrating Radar Data

Marie E. Fishel
Phillip T. Koehn

IDA

The Institute for Defense Analyses is a non-profit corporation that operates three federally funded research and development centers to provide objective analyses of national security issues, particularly those requiring scientific and technical expertise, and conduct related research on other national challenges.

Comparisons of Ring Resonator Relative Permittivity Measurements to Ground Penetrating Radar Data

Marie Fishel, Phillip Koehn

Institute for Defense Analyses, 4850 Mark Center Drive, Alexandria, VA 22311

ABSTRACT

Field experience has shown that soil conditions can have large effects on Ground Penetrating Radar (GPR) detection of buried targets of interest. The relative permittivity of the soil determines the attenuation of the radar signal. The contrast between the relative permittivity of the soil and the target is critical in determining the strength of the reflection from the target. In this paper, a microstrip ring resonator is used to measure the relative permittivity of the soil and various target fill materials. For this measurement technique, a microstrip ring resonator is placed in contact with a material medium and the real and imaginary parts of the relative permittivity are determined from changes in resonant frequencies (between 600 MHz and 2 GHz) and the quality factor of the resonator, respectively. Measurement results are compared to data collected by a GPR.

Keywords: ring resonator, ground-penetrating radar, permittivity**,** dielectric constant, soil

1. INTRODUCTION

For accurate field testing of GPR systems it is crucial to organize a test with relevant targets in realistic conditions. These conditions refer to the soil in which a target is buried, the depth at which the target is buried, and target configurations which will likely be encountered in theater. It is well known that soil conditions directly affect radar performance and thus it is desirable to measure the relative permittivity of the soil in-situ at the test site location. Permittivity depends on the moisture content of the soil as well as the soil type, thus these values will vary by location. Often during mathematical modeling or algorithm development for a GPR system, assumptions are made to simplify the problem. One such assumption is that the soil properties for each test site are the same. In this paper we analyze permittivity samples taken at locations spread throughout a small test site and illustrate that this assumption is invalid due to varying soil conditions. GPR data collected at the same locations will also be examined. By measuring the relative permittivity of the soil and fill materials used in targets of interest, analysts can better understand the strength of the GPR response and overall expected system performance in similar conditions.

2. PERMITIVITY CALCULATIONS USING RING RESONATOR DATA

The ring resonator utilizes ring antennas of varying frequencies to take measurements of the two port transmission coefficient. This coefficient is measured from the input feedline to the output feedline of the ring resonator antenna and denoted as $|S\_21|$. The transmission coefficient reaches a maximum value at the fundamental resonant frequency of the ring resonator antenna being used and all integer multiples of the fundamental frequency. To calculate the relative permittivity of a sample, the $|S\_21|$ waveforms of an air sample and a sample of a medium are compared. Permittivity is determined by changes in the location and widths of the resonance peaks when the antenna is in contact with a sample versus when the antenna is measuring the air. Figure 1 shows $|S\_21|$ waveforms using the 1200 MHz antenna for an air measurement and a measurement of a soil sample.
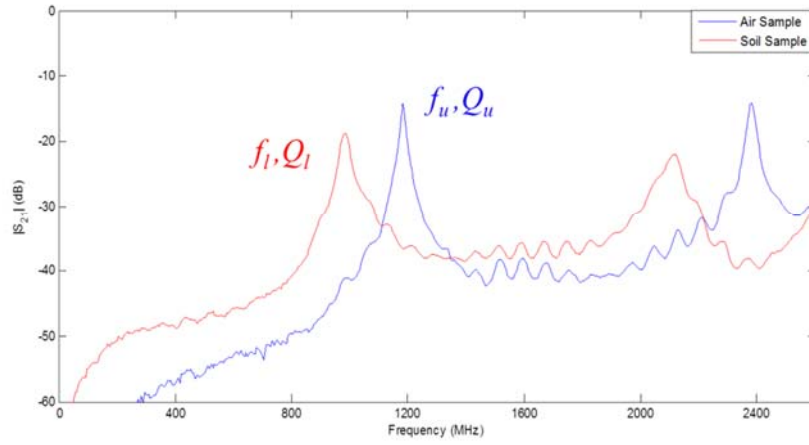
Figure 1: |S_21| values for an air sample and a soil sample

Since these measurements were taken with the 1200 MHz ring resonator antenna, the frequency at the resonant peak of the air sample (f_u) is 1200 MHz and the second resonant peak is at 2400 MHz. The quality factor or width of the peak of the resonance of the air sample is noted by Q_u. However, one can see that once the ring resonator antenna is placed in contact with the soil sample the resonant frequency shifts and the quality factor of the resonant peak is wider. The shift in the peak of the resonant frequency corresponds to the real part of the permittivity and the widening of the peak of the resonance corresponds to the imaginary part of the permittivity. Figure 2 shows how the real and imaginary parts of the permittivity are obtained from the ratio of the resonant frequencies and quality factors.
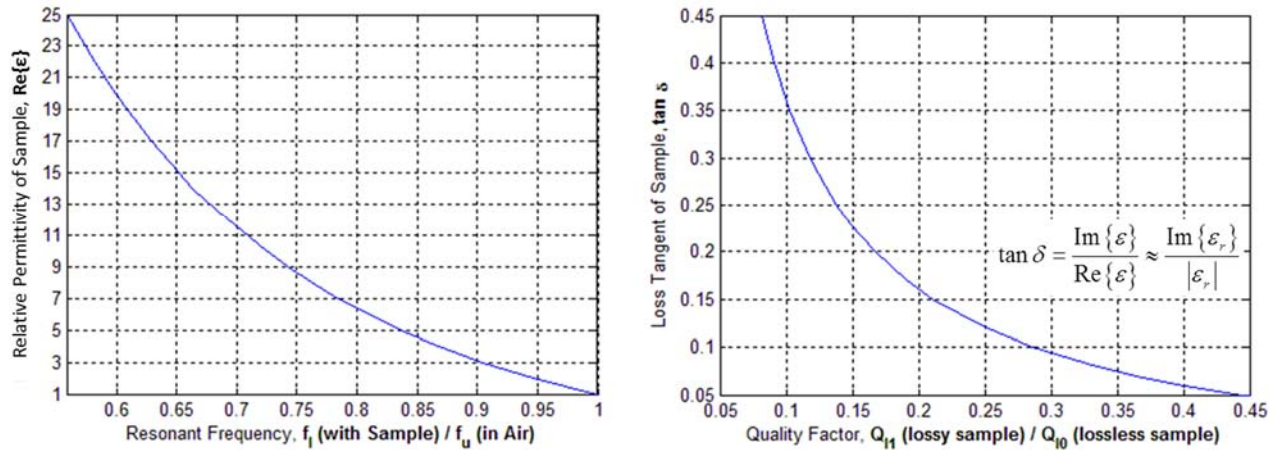

Figure 2: Calculating permittivity from the resonant frequency and quality factor ratios[1]

The left figure shows how the real value of the permittivity is obtained from the ratio of resonant frequencies of a soil sample and an air sample. This plot indicates that if a sample has a large shift in resonant frequency then the sample will have a high real permittivity. In the plot on the right, the ratio of the quality factor of a soil sample and air sample are related to the loss tangent. The equation on the plot describes the relationship between loss tangent and the imaginary part of the permittivity. This plot illustrates that if a soil sample has a much wider resonance peak than the air sample, then the imaginary part of the permittivity will be high.

In this paper, permittivity will be normalized by the permittivity of free space (ε_o) given by the equation:

$$\varepsilon_r = \frac{\varepsilon}{\varepsilon_o} = \frac{Re\{\varepsilon\}}{\varepsilon_o} + j\frac{Im\{\varepsilon\}}{\varepsilon_o} = Re\{\varepsilon_r\} + j * Im\{\varepsilon_r\}$$

ε_r is commonly referred to as the relative permittivity.

To attain values for ε_r from the measured |S_21| values, the resonant frequency and quality factor are found by least-squares fitting a Lorentzian curve to the data. Initial values for the fit parameters of amplitude, resonant frequency, and quality factor are the maximum value of the measured |S_21| value, the frequency at which the maximum value occurs, and the points at which the measured |S_21| values are 3 dB lower than the measured peak, respectively. To optimize these parameters and obtain a best fit curve, each parameter is swept over a small range of values. The measured data trace is subtracted from each of the fits from varying the parameters to form an error magnitude. The combination of parameter values for amplitude, resonant frequency, and quality factor that minimize the error are the values for the best Lorentzian fit. This procedure is performed for both the air sample measurement and the sample present measurement to obtain the values for f_l, Q_l, f_u, and Q_u (labeled in figure 1). A series of lookup tables were used to determine the real and imaginary values for ε_r. The lookup tables were generated by repeated simulations for each of the fabricated ring resonator antennas using a range for values for the real and imaginary permittivity for a simulated sample.[2]

3. RING RESONATOR FUNDAMENTALS

The microstrip ring resonator is a tool to measure the real and imaginary permittivity of soil samples in-situ, rather than requiring samples to be extracted and examined in a laboratory environment which would disturb the natural state of the soil. The ring resonator gets its name from the ring antenna which is part of a two-port transmission line structure. This structure contains an input and output feedline, a closed loop, and two coupling gaps. The ring resonates when the wavelength of Radio-frequency (RF) energy propagating in the transmission line is equivalent to the circumference of the ring.

The ring resonator used for this data collection was designed by the Army Research Laboratory (ARL)[3]. The developers created several ring resonator antennas that resonate at frequencies of 250, 1200, 1300, 1400, 1500, and 2000 MHz which were fabricated using copper traces on Rogers 4350B substrate. Figure 3 shows a typical ring resonator antenna corresponding to 1200 MHz.
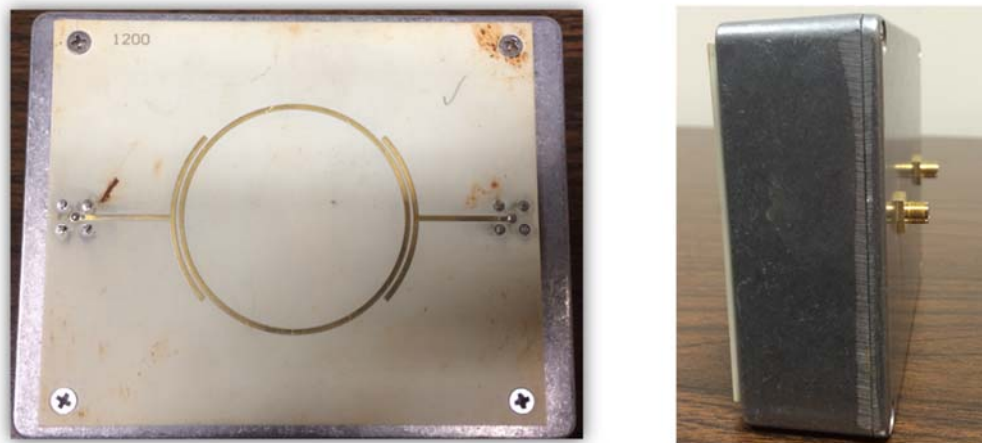

Figure 3: Front and side view of the 1200 MHz ring resonator antenna

Figure 3 consists of a front view and side view of the 1200 MHz antenna. In the front view, one can see the resonating ring and transmission line structure of the antenna. This part of the antenna is placed in contact with a medium to measure the real and imaginary permittivity. The side view image shows the connections on the back of the antenna which are connected via SMA cables to a network analyzer. A user utilizes the Agilent N9923A Vector Network Analyzer as an interface to the ring resonator when taking measurements.

Prior to taking measurements, the ring resonator must be calibrated. The full calibration details can be found in the ring resonator manual[3], but the short version will be explained here. To calibrate the system, the user performs a calibration of the network analyzer using a tool provided in port one of the network analyzer to measure a load, open, and short. The final calibration step is to connect ports one and two of the network analyzer using the SMA cables. Once all of the above steps have been measured, the system is ready to make measurements.

The user then interfaces with the network analyzer to determine the data type, sweep range, and resolution of the waveforms to be viewed. Prior to taking a measurement of the medium of interest, an air sample must be taken. This is done with the antenna pointing to the air with no medium nearby. After the no sample measurement is saved, the antenna is placed in contact with the medium of interest. When taking this measurement, pressure should be applied to the antenna to ensure full contact between the antenna and medium without any air gaps. If there are air gaps present when taking measurements, the resulting calculations for the permittivity of the medium will be incorrect. Specifically, the measured permittivity of the medium could be artificially lowered because the permittivity of air is also being measured and the real permittivity for air is 1. Figure 4 shows the ring resonator system configuration for an air sample measurement and a measurement of a slab of RTV, a mine fill simulant. Also pictured is a keyboard which is connected to the network analyzer via a USB port. The keyboard enhances the user interface with the network analyzer by allowing the user to type in the names for each file when saving measurements.
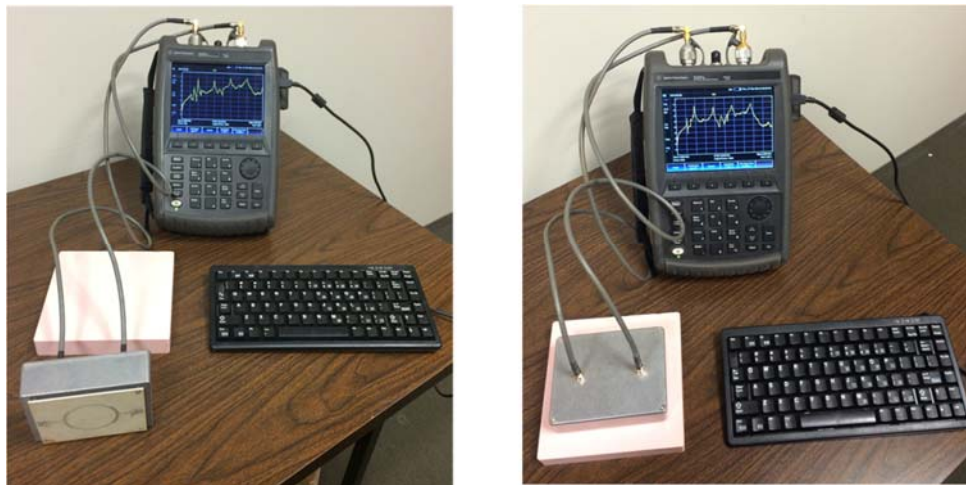

Figure 4: Ring resonator system set up for an Air Sample Measurement and a Measurement of RTV

Though the ring resonator is a very useful tool for measuring permittivity values in the field without disturbing the sample of the medium, it also has limitations. The primary limitation is that the ring resonator antenna must be completely flush with the medium to take an accurate measurement. While this may seem like a minor inconvenience, it can be difficult to attain good contact between the antenna and soil samples with different consistencies. Even soils that are mostly composed of sand or clay can still be rocky, which will reduce the contact between the antenna and soil. When taking measurements at different depths, you must ensure that the bottom of the hole is completely flat and free of rocks, which can be very difficult in many soil types.

To account for variations in soil grain sizes within one sample, it is best practice to take multiple measurements at each measurement location and average the results to attain realistic permittivity values for that location. For the measurements taken for this paper, we took five measurements at each sample location and rotated the orientation of the antenna slightly for each consecutive sample.

It is also best practice to press down on the antenna while taking a measurement to reduce any remaining air gaps and ensure flush contact between the antenna and the soil. Figure 5 shows the ring resonator taking a measurement on a sample of RTV without any pressure applied and with the user pressing down on the antenna while taking the measurement. In the left figure there is no pressure applied to the antenna while a measurement of the RTV is taken, while in the right figure, pressure is applied. The waveforms shown on the Network Analyzer in both figures are similar, with resonant peaks at 1200 MHz and all subsequent harmonics. However, if you look closely at the figure on the right, there is less noise in the waveform as a result of adding pressure to the antenna and reducing the air gaps present at the time of the measurement.
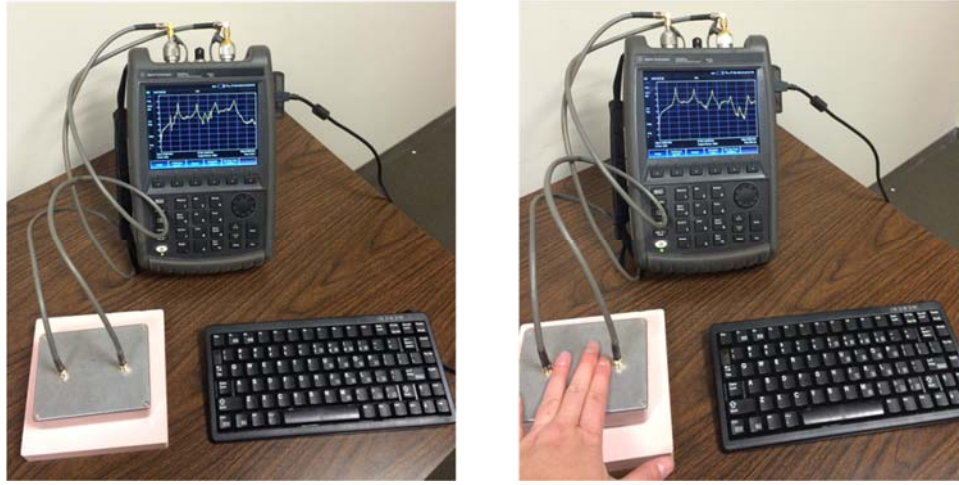
Figure 5: Taking a ring resonator measurement of RTV before and after applying pressure

In figure 6, we see the difference in the waveform of the RTV sample when pressure is applied. In the left figure, no pressure is applied while the measurement is taken and the waveform tends to mimic the air sample waveform. This indicates that if no pressure is applied while a measurement is taken, the resulting measurement will be a mixture of the sample and air. In the right figure, pressure is applied while the measurement is taken which results in the waveform being less noisy and having a larger shift in the resonant frequency as well as widening of the peak of the resonant frequency. This indicates that applying pressure to the antenna while taking a measurement is necessary to ensure that the measurement being taken is of the sample only, not a mixture of an air gap and the sample.
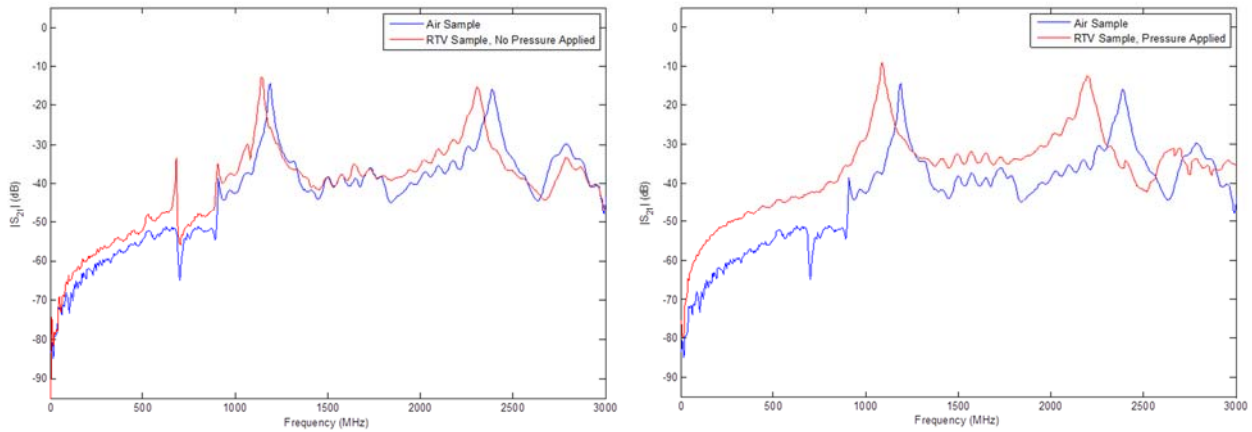

Figure 6: |S_21| values for an air sample and RTV sample with and without pressure applied

4. GPR DATA FUNDAMENTALS

GPR data was collected at the same locations and at nearly the same times as a set of ring resonator measurements, which is imperative to understanding the effect of soil conditions on GPR performance. GPR data was collected at various locations over targets of interest which were buried at different depths. The GPR system utilized for this data collection was the AN/PSS-14 handheld detector swung by an expert operator. Expert operators of the AN/PSS-14 have a specific methodology for collecting data which is shown in Figure 7.
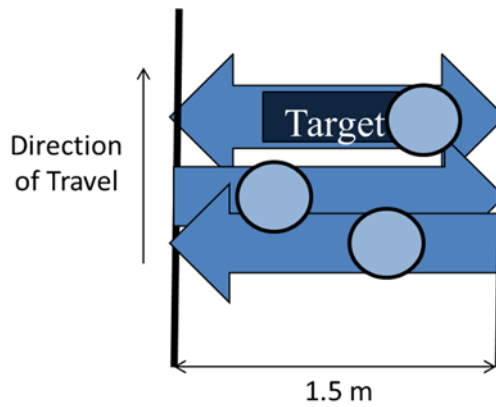
Figure 7: Handheld Data Collection Methodology

The thick black lines in figure 7 are the lane boundaries and the circle is representative of the detector head of the AN/PSS-14. First the operator sweeps back and forth over blank ground just before the location of the target to get a measure of what the background looks like near this target of interest. The operator then swings the detector back and forth over the target and uses a Trimble unit to press a button that sets a bit in the data stream to signify when the sensor head is directly over the target. Since handheld detectors do not employ any type of GPS system, the operator button press is vital for data analysis since there is no other way to determine when the detector is over the target.

The fundamental response of any GPR system is the A-scan, which is the amplitude of the GPR return as a function of time.[4] Handheld GPR A-scans are associated with a particular channel and a particular packet number. Figure 8 shows an A-scan response, collected over a buried metallic target. The largest response is from the ground, followed by two distinct high-magnitude reflections from the target itself.
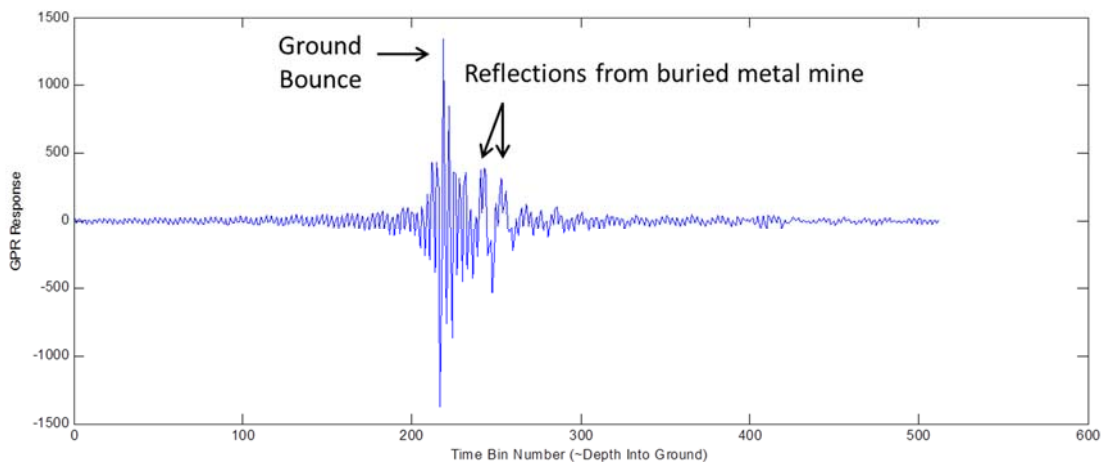

Figure 8: GPR A-Scan for a buried metal mine

If we rotate A-scans 90 degrees, plot A-scans side by side in successive time bins, and map the GPR responses values to a gray-scale image we create a B-scan. In B-scan images, the peaks and valleys of the GPR responses have been mapped to a color on the gray-scale color bar, with white being a high magnitude peak, and black being a high magnitude valley. We observe that the metallic target manifests itself as a parabola in this B-scan view of the GPR data.

In figure 9, processing has been applied to the GPR data to remove the response due to the ground. In the B-scan we can see that most of the ground response has been removed but there are some spots of residual ground response. The ground bounce removal processing will be applied to all GPR data analyzed in this paper. The B-scan in has dimensions of time bins by packet numbers and corresponds to the data from channel 1 of the GPR. Since the handheld detector collects data in continuous packets, the B-scan contains several responses to the buried metal mine as the operator swings back and forth over the target.
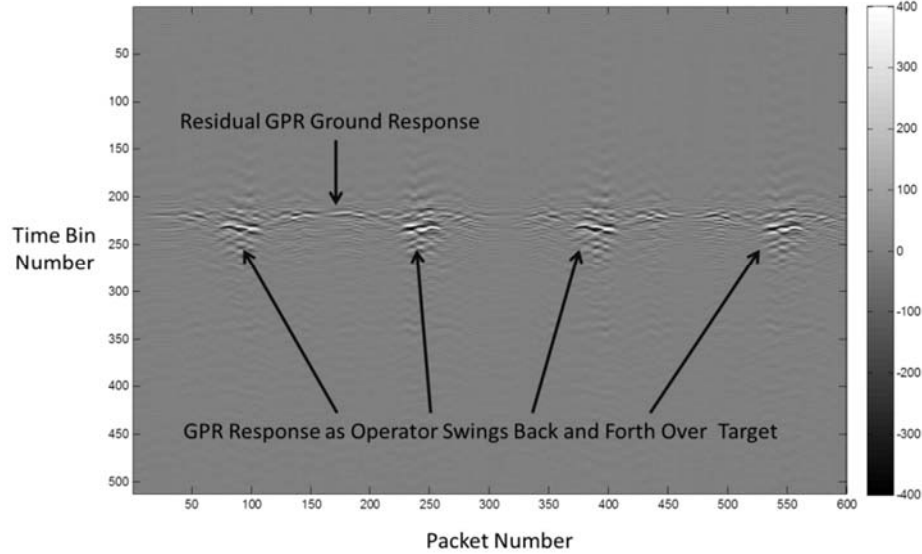

Figure 9: GPR B-Scan for a buried metal mine

Soil properties such as conducitvity, magnetic permeability, and permittivity affect how GPR waves propagate and attenuate in the soil and thus these properties are key to understanding GPR performance against targets. Since these properties can vary within a test site or even within a particular lane of the test site, targets that are buried in one location may have different GPR responses than the same target buried in another location. This is because the reflection loss of a GPR wave hitting a target and reflecting back is directly dependant on the contrast in magnetic permeability and permittivity of the target and surrounding soil. If the target and surrounding soil have very similar permeability and permittivity values, then the target will be difficult to detect for the GPR. The equation for the reflection loss, assuming normal incidence of a plane wave is given by:

$$R = \frac{\sqrt{\frac{\mu_s * \varepsilon_t}{\mu_t * \varepsilon_s}} - 1}{\sqrt{\frac{\mu_s * \varepsilon_t}{\mu_t * \varepsilon_s}} + 1}$$

In the above equation for reflection loss, μ_s and ε_s correspond to the magnetic permeability and permittivity of the soil, while μ_t and ε_t correspond to the magnetic permeability and permittivity of the target.[5]It is useful to convert the reflection loss into units of decibels which can be done by utilizing the equation:

$$R_{dB} = 20 \log_{10}(R)$$

Attenuation refers to how much energy is lost in the soil as the GPR wave passes through it. The equation for attenuation loss in dB per meter depends on frequency, conductivity, permittivity, and permeability and is given by

$$\eta = 20 \log_{10}(e^{\frac{\omega}{c}\sqrt{\frac{\sqrt{A^2+B^2}-A}{2}}})$$

where: A = $\text{Re}\{\mu_r\}*\text{Re}\{\varepsilon_r\}-\text{Im}\{\mu_r\}(\text{Im}\{\varepsilon_r\} + \frac{\sigma}{\omega\varepsilon})$, B = $\text{Im}\{\mu_r\}*\text{Re}\{\varepsilon_r\}+\text{Re}\{\mu_r\}(\text{Im}\{\varepsilon_r\} + \frac{\sigma}{\omega\varepsilon})$, c = $\frac{1}{\sqrt{\varepsilon_0\mu_0}}$, and $\omega = 2\pi f$.

In the equation for attenuation, μ_r and ε_r correspond to the relative magnetic permeability and permittivity of the soil, σ is the conductivity of the soil, and μ_0 and ε_0 correspond to magnetic permeability and permittivity of free space.[6]

5. RING RESONATOR AND GPR DATA COLLECTION

Ring resonator and GPR data were collected on the calibration lanes at a tropical test site in January 2014. Both sets of data were collected twice, once on the morning of January 21 and once in the afternoon on January 23. Significant rainfall occurred between the two days of data collection. Both sets of measurements were collected at thirteen locations spread across seven calibration lanes. Figure 10 shows the layout of the calibration handheld test lanes and the data collection locations indicated by the blue numbered boxes.
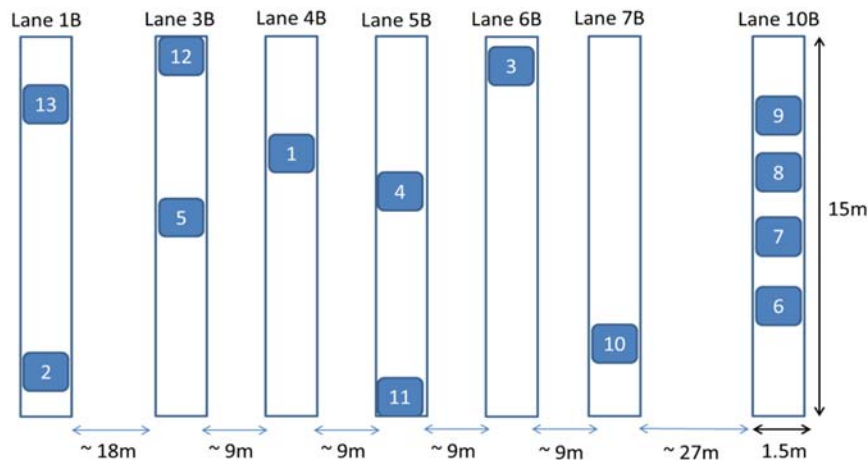

Figure 10: Ring resonator and GPR data collection locations at Schofield Barracks

All lanes are relatively flat and straight with terrain that is a combination of grass and dirt. Lanes 7B and 10B are located on slightly higher ground and therefore dried out quicker than the other lanes after the significant rainfall on January 22. These lanes also tended to have less vegetative coverage. Water tended to collect the most in lanes 4B, 5B, and 6B which had the most vegetative growth. Figure 10 contains photos of two different locations where measurements were taken on January 23, after the significant amount of rainfall.
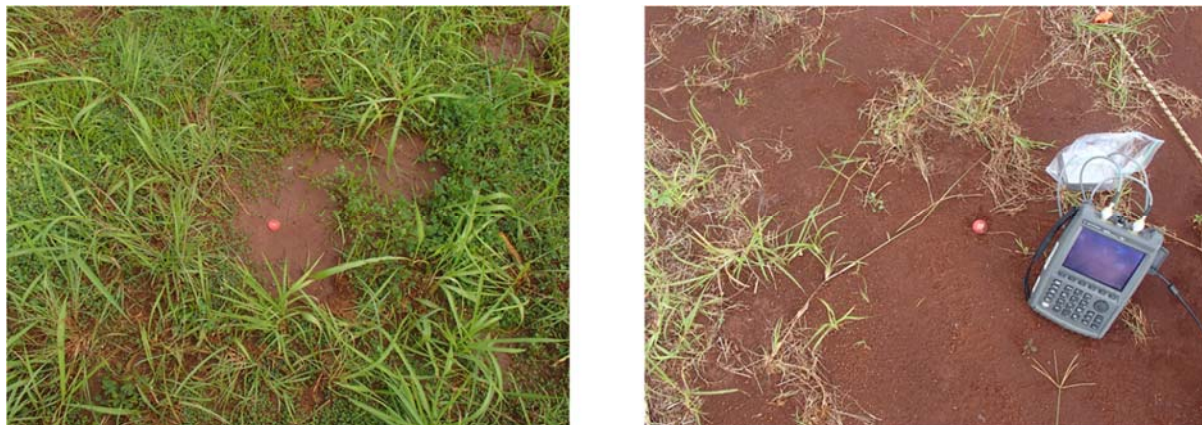

Figure 11: Photos of measurement locations number 1 and 10

The photo on the left in figure 11 corresponds to data collection location number 1, which is located in lane 4B. This location is surrounded by vegetation and is muddy due to the rainfall. Also note that there is a visual indicator at this location, the grass does not grow at the location of the buried target.

The photo on the right in figure 11 corresponds to data collection location number 10, which is located in lane 7B. Lane 7B is on higher ground and thus there is not as much vegetation at this location and the ground is much less muddy. Also, the ring resonator is set up in this photo as we prepare to take in-situ permittivity measurements at this location. The ring resonator is inside a plastic bag to protect the antenna from the muddy soil at the various measurement locations.

6. RESULTS

The ring resonator and GPR data was analyzed upon return to IDA and the real and imaginary part of the permittivity, as well as the loss tangent was calculated for all measurements. As expected, the permittivity values for most locations were higher on January 23rd than January 21st due to the significant rainfall that fell between those days. The permittivity value increases after rainfall because water has a relative permittivity of 80 and thus when the soil is saturated with moisture, the permittivity will increase. Since the elevation of the lanes differed, those that were located slightly downhill were more susceptible to the effect of the rainfall, since water collected here and these lanes did not dry as quickly. The permittivity values were not consistent throughout the site, or even within the same lane. Figure 12 shows the real and imaginary permittivity and loss tangent values at various down-track locations in Lane 10B.
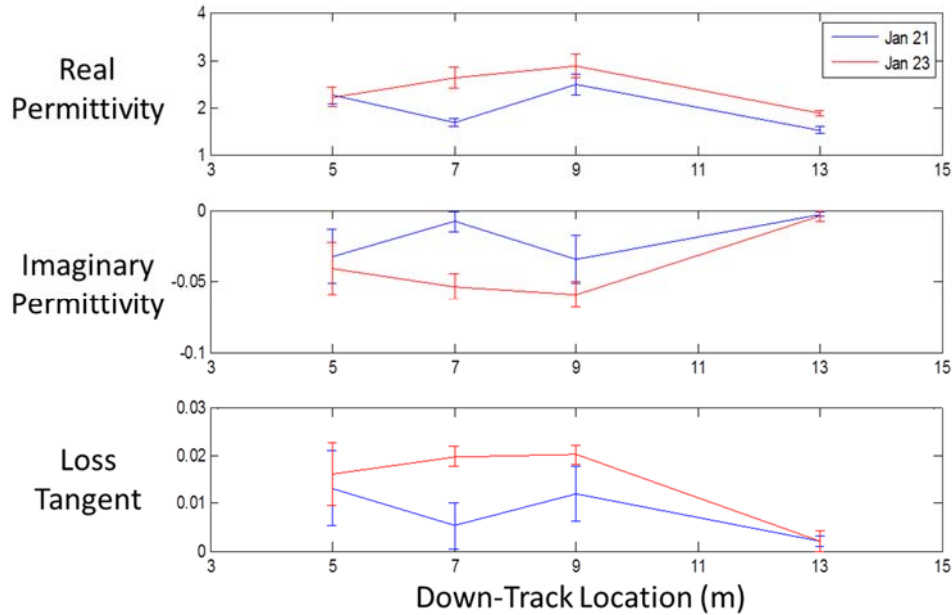

Figure 12: Permittivity and loss tangent values as a function of down-track location in Lane 10B

Down-track location as referred to in figure 12 refers to the number of meters down the length of the 15 meter lane beginning with the end of the lane that is on the bottom of figure 10. Thus, the 5, 7, 9, and 13 meter down-track measurements correspond to measurement locations numbered 6, 7, 8, and 9, respectively.

From figure 12, it can be observed that the 5 meter down-track location was more immune to the effects of the heavy rainfall than the rest of the locations in Lane 10B since values for the real and imaginary permittivity and the loss tangent are statistically the same for both measurement days. The 9 meter down-track location had the highest real permittivity values for both measurement days and was statically higher than all other measurement locations on January 21. The 9 meter down-track location also has statistically higher values for the real permittivity and loss tangent than the 13 meter down-track location on both measurement days. This result is significant because it illustrates the variation in soil that can occur not only at the same site, but within the same lane. Two locations located 4 meters a part down-track and with little across-track displacement have significantly different soil properties which affect target detection.

All down-track locations in lane 10B which are plotted in figure 12 contain the same target. This target is buried at a shallow depth at locations located 5 and 9 meters down-track and at a deeper depth at locations 7 and 13 meters down-track. The target present at all locations in lane 10B has a fill with Re$\{\varepsilon_r\}$ equal to 2.2 and Imag$\{\varepsilon_r\}$ equal to -0.012. These values were used to calculate the attenuation loss, reflection loss, and total loss for all down-track locations in lane 10B using the equations from section 4. Table 1 contains the calculated values with Attenuation Loss in dB, which is attained by multiplying η, which has units of dB/m, by twice the depth of the target to account for attenuation due to the full path of travel. Total loss is simply the addition of attenuation loss and reflection loss.

Table 1: Attenuation and reflection loss calculations for the target at all locations in lane 10B

Location (m)	January 21			January 23		
	Attenuation Loss (dB)	Reflection Loss (dB)	Total Loss (dB)	Attenuation Loss (dB)	Reflection Loss (dB)	Total Loss (dB)
5	-0.57	-41.98	-42.55	-0.69	-41.53	-42.21
7	-0.66	-23.01	-23.67	-1.55	-27.67	-29.22
9	-0.57	-30.89	-31.46	-2.74	-23.13	-25.86
13	-0.38	-20.40	-20.78	-0.43	-27.13	-27.56

Though down-track locations 5 and 9 meters are encounters of the same target at the same depth, the reflection loss and total loss at the two locations are quite different. The measured permittivity at 5 meters down-track is nearly equivalent to the permittivity of the target fill, thus the contrast in permittivity between the soil and target fill is minimal and the reflection loss is high. As mentioned before, the 5 meter down-track location was immune to the effects of the heavy rainfall and thus there was almost no change in permittivity or reflection loss between the two measurement dates. The 9 meter down-track location had the highest real permittivity on both measurement dates and thus the contrast between the soil and target fill at this location was more significant which resulted in a much lower reflection loss than the 5 meter down-track location.

We now examine the permittivity and loss tangent values for two different places within the site that contain the same metal mine test target buried *at the same depth*. One encounter of this target is at measurement location number 2, located at the beginning on Lane 1B, while the other encounter of this target is at measurement location number 3, located at the end of Lane 6B. Figure 13 shows the permittivity and loss tangent values measured at each location on both days.
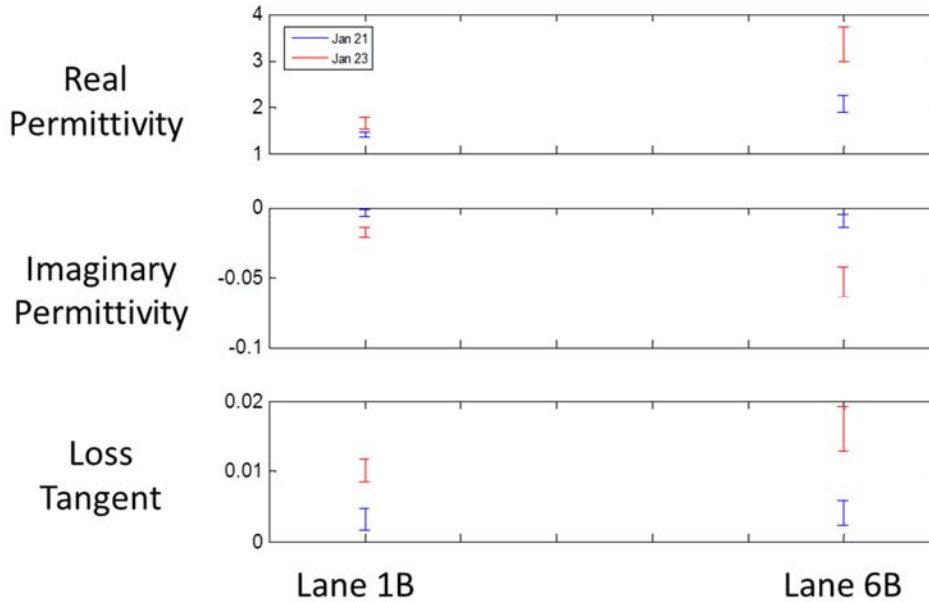

Figure 13: Permittivity and loss tangent values for the two different locations of the same target

In figure 13 we see the same trend as before, where the location in Lane 1B is more immune to the effects of heavy rainfall than Lane 6B. It is interesting to note that the real values of the permittivity are significantly different between the two locations on both measurement days. Next we examine the effect that the significantly different permittivity values have on the GPR response of this target by examining the attenuation and reflection loss. Table 2 contains the calculated attenuation, reflection loss, and total loss for both locations on both measurement dates.

Table 2: Attenuation and reflection loss calculations for the same target at two different locations

Location	January 21			January 23		
	Attenuation Loss (dB)	Reflection Loss (dB)	Total Loss (dB)	Attenuation Loss (dB)	Reflection Loss (dB)	Total Loss (dB)
Lane 1B	-0.12	-21.86	-21.98	-0.31	-18.2	-18.51
Lane 6B	-0.23	-15.05	-15.28	-0.50	-10.74	-11.24

Since the estimated permittivity of the test target is low, there is less reflection loss at both locations on January 23 compared to January 21. Recall that significant rainfall occurred between these two dates, which increased the measured permittivity at both locations. This resulted in better contrast in permittivity between the target and the soil, which yielded less reflection loss. The target location in lane 6B was less immune to the effects of heavy rainfall and thus permittivity significantly increased, resulting in a significant drop in reflection loss. However, negative effects of moisture at this location can be seen in the attenuation loss, which increases after the heavy rainfall. The total loss decreases for both locations after the rainfall, which indicates the advantage of lower reflection loss outweighs the increased attenuation loss resulting from increased permittivity due to rainfall. Since the reflection loss decreases due to the increased contrast in permittivity between the soil and target after rainfall, the GPR response corresponding to the target at these locations should be stronger after the rainfall. We will now examine B-scans of the target at each location before and after rainfall to determine if the strength of the GPR response correlates with the calculated reflection loss and total loss.
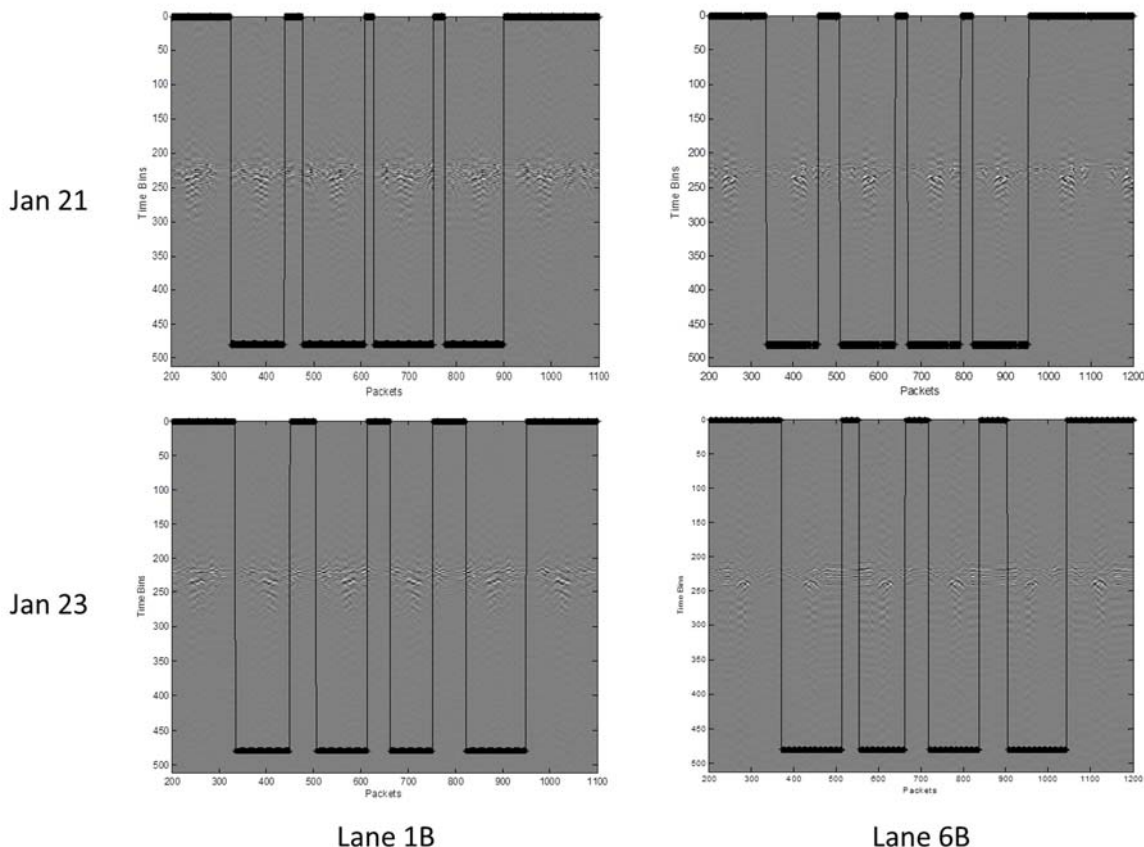
Figure 14: GPR B-scan response for the same target at two locations, before and after rainfall

In the B-scans in figure 14, the black line corresponds to the packet numbers during which the operator has pressed the button on the data collection unit, indicating that they believe they are swinging over the target location. Recall that the operator will swing back and forth over the target and press a button on the data collection unit while over the target. Thus, the GPR responses due to the buried metal mine tend to be centered inside the black lines. The top two B-scans in figure 14 correspond to GPR data taken on January 21 and the bottom two B-scans correspond to GPR data taken on January 23, after the significant rainfall.

These B-scans are from two instances of the same target at the same depth, one encounter of the target is located in lane 1B and the other is in lane 6B. It can be observed that even though the B-scans correspond to the same target at the same depth, the GPR response is stronger for the target located in lane 6B for both dates. This observation is expected since the reflection loss and total loss calculated for lane 6B are lower on both measurement dates than those calculated for lane 1B. One can also notice that the GPR response to the target located in lane 1B seems stronger in the data taken January 23, compared to the data taken January 21. This phenomenon should also be expected, since the reflection loss and total loss decreased after the significant rainfall due to the increased contrast in permittivity between the target and soil.

Figure 15 shows the B-scans for the target locations in lane 1B and lane 6B on January 23, after the significant rainfall. These B-scans have been zoomed in such that only time bins 150 through 300 are plotted and the response due to the target can be more easily seen. The black vertical lines in these B-scans correspond to the button press areas. The GPR response to the target located in 6B is stronger and easier to pick out of the background than the location in lane 1B. The hyperbolic shape of the target is more evident in lane 6B as well.
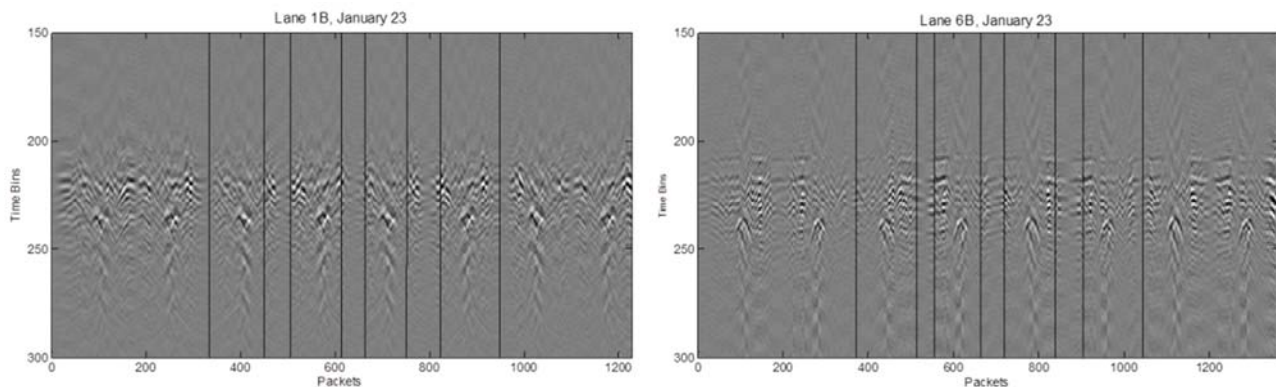

Figure 15: Zoomed in view of GPR B-scans of a target at two locations

To quantify the strength of the GPR response in the B-scan we can examine the output from the GPR anomaly metric, which is an algorithm that runs on the AN/PSS-14 and relies solely on the GPR response. Detections by the GPR anomaly metric occur when the metric value is higher than a threshold. The threshold for the GPR anomaly metric is adaptive and dependent on the constantly updated background model of the AN/PSS-14. Figure 16 shows plots of the normalized GPR anomaly metric and corresponding normalized threshold for both encounters of the target in lane 1B and 6B on both measurement dates.

The peaks in the plots in figure 16 correspond to the packet numbers during which the handheld detector was over the target. The button press lines are not plotted here due to the difference in swing between measurement dates on lane 6B, which resulted in the detector being over the target in differing packet numbers. However, the four center peaks for each plot correspond to the location of the operator button press. Recall that all GPR responses plotted in figure 16 correspond to the same target at the same depth, but located in two different lanes.
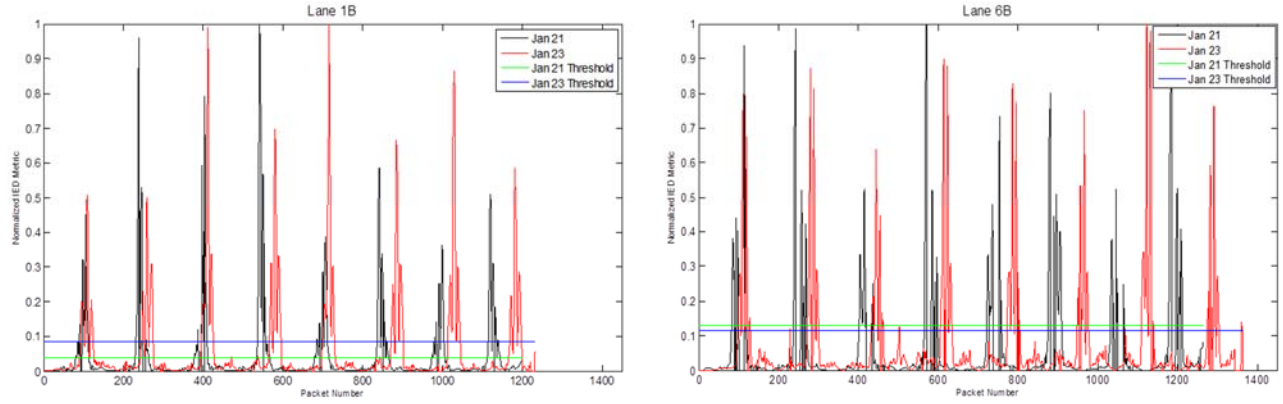
Figure 16: Normalized GPR anomaly metric for both target encounters on both measurement dates

If we compare the GPR response between the two target locations, we see that there is more overall GPR response due to the target located in lane 6B. This is evidenced by the width of the large peaks of GPR response over the target being larger and wider in lane 6B compared to those in 1B. The reflection loss and total loss calculations in table 2 show that the target location in lane 6B has consistently lower loss values than the target location in lane 1B, thus we would expect the GPR return from the target location in 6B to be larger.

To quantify the GPR response we can take a weighted sum of the Normalized GPR anomaly metric values for all packets where the response has exceeded the normalized threshold and divide this sum by the total number of packets during which the GPR anomaly metric was above threshold. Table 3 contains the weighted average normalized GPR anomaly metric value for both locations on both measurement dates.

Table 3: Weighted average normalized GPR anomaly metric values

Location	Weighted Average	
	January 21	January 23
Lane 1B	0.20	0.28
Lane 6B	0.33	0.36

The weighted average values of the normalized GPR anomaly metric confirm the observations from examining the B-scans in figures 14 and 15. The response to an identical target at the same depth is stronger at the target location in lane 6B than the location in lane 1B for both measurement dates. From the reflection loss values in table 2, we expect that the GPR response to the target would be larger after the rainfall due to the moisture in the soil increasing the real permittivity which results in a larger contrast between the target and the soil. Table 3 shows that the weighted average for normalized GPR anomaly metric value is larger at both locations on the January 23 compared to January 21.

7. CONCLUSIONS AND FUTURE WORK

Understanding the soil conditions such as permittivity and magnetic permeability is vital to understanding the GPR response to targets of interest. The ring resonator is a useful tool that enables an analyst to measure the permittivity of the soil at a test site without disturbing the soil sample. Using this tool, it is clear that the permittivity varies within a test site or even within the same lanes at a test site. These variations in permittivity and other soil conditions directly impact the GPR response due to targets since the reflection coefficient is directly dependent on the contrast between the permittivity and permeability of the target and the soil. Thus, identical targets buried at the same depth in different areas of the site or even with a down-track separation within the same lane can have very different GPR responses.

Future work for this analysis includes collecting permittivity samples at test sites with different soil conditions under various environmental conditions. This data was collected at Schofield Barracks before and after significant rainfall. It is of interest to collect samples at Yuma Proving Ground in Arizona and Fort AP Fill in Virginia under dry and wet conditions to determine what impact soil moisture has at these sites. When additional data is collected, it is also desirable to collect soil moisture measurements and GPR data at the same locations so that the impact on target detection could be evaluated.

8. REFERENCES

1. Mazzaro, G., Sherbondy, K., Smith, G., Harris, R., Sullivan, A., "Characterization of Dielectric Materials using Ring Resonators", *U.S. Army Research Laboratory Technical Advisory Board Demonstation,* May 2011.
2. Mazzaro, G., "In-Situ Permittivity Measurements using Ring Resonators", *Proceedings of SPIE 8361*, April 2012.
3. Mazzaro, G., Sherbondy, K., Smith, G., Ressler, M., Harris, R., "Portable Ring-Resonator Permittivity Measurement System: Design & Operation", *U.S. Army Research Laboratory Technical Report,* Dec.2011.
4. Jackson, J. D. (1962, 1975, 1998). *Classical Electrodynamics, pp282*
5. Daniels DJ 2004, *Ground Penetrating Radar 2nd Edition*, The Institution of Engineering and Technology
6. Stillman, D. and Olhoeft, G., "Frequency and temperature dependence in electromagnetic properties of Martian analog minerals," *Journal of Geophysical Research* Volume 113.

REPORT DOCUMENTATION PAGE

1. REPORT DATE	2. REPORT TYPE	3. DATES COVERED *(From–To)*
April 2014	Final	December 2013 – March 2014

4. TITLE AND SUBTITLE	5a. CONTRACT NUMBER
Comparison of Ring Resonator Relative Permittivity Measurements to Ground Penetrating Radar	W91WAW-09-C-0003
	5b. GRANT NUMBER
	5c. PROGRAM ELEMENT NUMBER

6. AUTHOR(S)	5d. PROJECT NUMBER
Fishel, Marie E. Koehn Phillip T.	
	5e. TASK NUMBER AK-2-1982
	5f. WORK UNIT NUMBER

7. PERFORMING ORGANIZATION NAME(S) AND ADDRESS(ES)	8. PERFORMING ORGANIZATION REPORT NUMBER
Institute for Defense Analyses 4850 Mark Center Drive Alexandria, VA 22311-1882	IDA Document NS D-5155 Log: H 14-000296

9. SPONSORING / MONITORING AGENCY NAME(S) AND ADDRESS(ES)	10. SPONSOR/MONITOR'S ACRONYM(S)
U.S. Army RDECOM CECOM Night Vision Electronic Sensors Directorate 10221 Burbeck Road Ft. Belvoir, VA 22060-5806	RDECOM CECOM/NVESD
	11. SPONSOR/MONITOR'S REPORT NUMBER(S)

12. DISTRIBUTION/AVAILABILITY STATEMENT

Approved for public release; distribution is unlimited (27 March 2014).

13. SUPPLEMENTARY NOTES

14. ABSTRACT

Field experience has shown that soil conditions can have large effects on Ground Penetrating Radar (GPR) detection of buried targets of interest. The relative permittivity of the soil determines the attenuation of the radar signal. The contrast between the relative permittivity of the soil and the target is critical in determining the strength of the reflection from the target. In this paper, a microstrip ring resonator is used to measure the relative permittivity of the soil and various target fill materials. For this measurement technique, a microstrip ring resonator is placed in contact with a material medium and the real and imaginary parts of the relative permittivity are determined from changes in resonant frequencies (between 600 MHz and 2 GHz) and the quality factor of the resonator, respectively. Measurement results are compared to data collected by a GPR.

15. SUBJECT TERMS

ring resonator, ground-penetrating radar, permittivity, dielectric constant, soil

16. SECURITY CLASSIFICATION OF:			17. LIMITATION OF ABSTRACT	18. NUMBER OF PAGES	19a. NAME OF RESPONSIBLE PERSON Navish, Frank
a. REPORT Uncl.	b. ABSTRACT Uncl.	c. THIS PAGE Uncl.	SAR	17	19b. TELEPHONE NUMBER *(include area code)* (703) 704-2886